

A Scaler-Based Data Acquisition System for Measuring Parity Violation Asymmetry in Deep Inelastic Scattering

R. Subedi ^{a 1}, D. Wang ^a, K. Pan ^b, X. Deng ^a, R. Michaels ^c,
P. E. Reimer ^d, A. Shahinyan ^e, B. Wojtsekhowski ^c, X. Zheng ^{a,*}

^aUniversity of Virginia, Charlottesville, VA 22904, USA

^bMassachusetts Institute of Technology, Cambridge, MA 02139, USA

^cThomas Jefferson National Accelerator Facility, Newport News, VA 23606, USA

^dPhysics Division, Argonne National Laboratory, Argonne, IL 60439, USA

^eYerevan Physics Institute, Yerevan, Armenia

Abstract

An experiment that measured the parity violating asymmetry in deep inelastic scattering was completed at the Thomas Jefferson National Accelerator Facility in experimental Hall A. From this asymmetry one can extract a combination of the quark weak axial charge. To achieve this, asymmetries at the 10^{-4} level need to be measured at event rates up to 500 kHz and the high pion background typical to deep inelastic scattering experiments needs to be rejected efficiently. A specialized data acquisition (DAQ) system with intrinsic particle identification (PID) was successfully developed and used: The pion rejection achieved was above $(1.6 \times 10^4) : 1$ with a higher than 91% electron efficiency throughout the experiment; The systematic uncertainty in the measured asymmetry due to DAQ deadtime was below 0.2%; And the statistical quality of the asymmetry measurement agrees with the Gaussian distribution to over five orders of magnitudes. The DAQ system is presented here with an emphasis on its design scheme, the achieved PID performance, deadtime effect and the capability of measuring small asymmetries.

Key words: Jefferson Lab; Hall A; PVDIS; DAQ

PACS: 11.30.Er, 12.15.Mm, 13.60.Hb 14.60.Cd 14.65.Bt 29.30.Aj 29.85.Ca

¹ Present address: George Washington University, 725 21st St, NW, Washington, DC 20052, USA

* Corresponding author. E-mail: xiaochao@jlab.org; Telephone: 001-434-243-4032; Fax: 001-434-924-4576

27 1 Introduction

28 The Parity Violating Deep Inelastic Scattering (PVDIS) experiment E08-011 was
 29 completed in December 2009 at the Thomas Jefferson National Accelerator Facil-
 30 ity (JLab). The goal of this experiment [1,2] was to measure with high precision
 31 the parity violating asymmetry in deep inelastic scattering of a polarized electron
 32 beam on an unpolarized liquid deuterium target. This asymmetry is sensitive to a
 33 combination of the quark weak axial charge $2C_{2u} - C_{2d}$, where $C_{2q} = 2g_V^e g_A^q$ with
 34 $q = u, d$ indicating an up or a down quark, g_V^e is the electron vector coupling and
 35 g_A^q is the quark axial coupling to the Z^0 boson.

36 For electron inclusive scattering from an unpolarized target, the electromagnetic
 37 interaction is parity conserving and is insensitive to the spin flip of the incom-
 38 ing electron beam. Only the weak interaction violates parity and causes a differ-
 39 ence between the right- and the left-handed electron scattering cross-sections σ_R
 40 and σ_L . The dominant contribution to the parity violation asymmetry, $A_{PV} \equiv$
 41 $(\sigma_R - \sigma_L)/(\sigma_R + \sigma_L)$, arises from the interference between electromagnetic and
 42 weak interactions and is proportional to the four momentum transfer squared Q^2
 43 for $Q^2 \ll M_Z^2$. The magnitude of the asymmetry is in the order of 10^{-4} or 100 parts
 44 per million (ppm) at $Q^2 = 1 \text{ (GeV/c)}^2$.

45 The PVDIS asymmetry from a deuterium target is

$$A_{PV} = \left(-\frac{G_F Q^2}{4\sqrt{2}\pi\alpha} \right) \left(2g_A^e Y_1 \frac{F_1^{\gamma Z}}{F_1^\gamma} + g_V^e Y_3 \frac{F_3^{\gamma Z}}{F_1^\gamma} \right), \quad (1)$$

46 where Q^2 is the negative of the four-momentum transfer squared, G_F is the Fermi
 47 weak coupling constant, α is the fine structure constant, Y_1 and Y_3 are kinematic
 48 factors, x is the Bjorken scaling variable, and $F_{1,3}^{\gamma(Z)}$ are deuteron structure functions
 49 that can be evaluated from the parton distribution functions and the quark- Z^0 vector
 50 and axial couplings $g_{V,A}^q$. From this asymmetry one can extract the quark weak
 51 vector and axial charges $C_{1,2q}$, which can be written as

$$\begin{aligned} C_{1u} &= 2g_A^e g_V^u = -\frac{1}{2} + \frac{3}{4} \sin^2 \theta_W, & C_{2u} &= 2g_V^e g_A^u = -\frac{1}{2} + 2 \sin^2 \theta_W, \\ C_{1d} &= 2g_A^e g_V^d = \frac{1}{2} - \frac{2}{3} \sin^2 \theta_W, & C_{2d} &= 2g_V^e g_A^d = \frac{1}{2} - 2 \sin^2 \theta_W, \end{aligned}$$

52 in the tree-level Standard Model with θ_W the weak mixing angle.

53 The goal of JLab E08-011 is to measure the PVDIS asymmetries to statistical pre-
 54 cisions of 3% and 4% at $Q^2 = 1.1$ and 1.9 (GeV/c)^2 , respectively, and under the
 55 assumption that hadronic physics corrections are small, to extract the quark axial
 56 weak charge combination $(2C_{2u} - C_{2d})$. In addition, the systematic uncertainty goal

is less than 3%. For this experiment, the expected asymmetries are 91 and 160 ppm respectively at the two Q^2 values. To achieve the required precision, an event rate capability of up to 500 kHz is needed.

The main challenge of deep inelastic scattering experiments is the separation of scattered electrons from charged pion background in the spectrometer and detector system. Charged pions are produced primarily from nucleon resonance decays and could carry a parity violation asymmetry corresponding to the Q^2 at which the resonances are produced, typically a fraction of the asymmetry of electrons with the same scattered momentum. Assuming a fraction f of the detected events are π^- and $1 - f$ are electrons, the measured asymmetry is

$$A_m = f A_\pi + (1 - f) A_e, \quad (2)$$

where A_e is the desired electron scattering asymmetry and A_π is the asymmetry of the pion background. To extract A_e to a high precision, one needs to either minimize the pion contamination f to a negligible level, or to correct the measured asymmetry for the asymmetry of pions, which itself needs to be measured precisely. For the PVDIS experiment, the goal was to reach $f < 10^{-3}$. Since the expected π to electron ratio varies between $(1 - 10) : 1$, a 10^4 pion rejection was needed.

The experiment used a 100 μ A electron beam with a polarization of approximately 90% and a 20-cm long liquid deuterium target. The two High Resolution Spectrometers (HRS) [3] were used to detect scattered events. While the standard HRS detector package and data acquisition (DAQ) system routinely provide a 10^4 pion rejection with approximately 99% electron efficiency, they are based on full recording of the detector signals and are limited to event rates up to 4 kHz [3]. This is not sufficient for the high rates expected for the experiment. (The HRS DAQ will be referred to as “standard DAQ” hereafter.)

Most previous parity violation experiments—SAMPLE [4] at MIT-Bates, HAPPEX [5–9], and PREX [10] at JLab – focused on elastic scattering from nuclear or nucleon targets that are typically not contaminated by inelastic backgrounds. Signals from the detectors can be integrated and a helicity dependence in the integrated signal can be used to extract the physics asymmetry, and no pion rejection was implemented. An integrating DAQ was also used at the preceding PVDIS measurement at SLAC [11,12] in which approximately 2% of the integrated signal was attributed to pions. In the Mainz PVA4 experiment [13–15], particles were detected in a total absorption calorimeter and integrated energy spectrum was recorded. Charged pions and other background were separated from electrons in the offline analysis of the energy spectrum, and the pion rejection is in the order of 100:1 based on the characteristics of the calorimeter.

High performance particle identification can usually be realized in a counting-based DAQ where each event is evaluated individually. In the G0 experiment [16–20] at

95 JLab, a superconducting spectrometer with 2π azimuthal angle coverage was used
 96 to detect elastically scattered protons at the forward angle and elastic electrons at
 97 the backward angle. At the forward angle, protons were identified using time-of-
 98 flight. At the backward angle, pions were rejected from electrons using an Aerogel
 99 Cherenkov counter and a pion rejection factor of 125 : 1 was reported. The dead-
 100 time correction of the counting system was at the order of a few percent.

101 While the PVDIS experiment can fully utilize existing spectrometers and detectors
 102 at JLab, upon examining all existing techniques for PV measurements it became
 103 clear that a custom electronics and DAQ were needed to control the systematic
 104 uncertainties due to data collection to below 1%. In this paper we describe a scaler-
 105 based, cost effective counting DAQ which limited the pion contamination of the
 106 data sample to a negligible level of $f < 10^{-3}$. Basic information of the detector
 107 package and the DAQ setup will be presented first, followed by analysis focused on
 108 electron detection efficiency, pion rejection, corrections due to counting deadtime,
 109 and the statistical quality of the asymmetry measurement.

110 2 Detector and DAQ Overview

111 The design goal of the DAQ is to record data up to 1 MHz with hardware-based PID
 112 and well measured and understood deadtime effects. The following detectors in the
 113 HRS were used to characterize scattered particles: Two scintillator planes provided
 114 the main trigger, while a CO₂ gas Cherenkov detector and a double-layer segmented
 115 lead-glass detector provided particle identification information. The vertical drift
 116 chambers (as the tracking detector) were used during calibration runs and turned
 117 off during production data taking because they were not expected to endure the
 118 high event rates.

119 For the gas Cherenkov and the lead-glass detector, a full recording of their output
 120 ADC data is not feasible at the expected high rate. Instead their signals are passed
 121 through discriminators and logic units to form preliminary electron and pion trig-
 122 gers. Particle identification is fulfilled by the use of discriminators for both the lead-
 123 glass and the Cherenkov detectors and proper settings of their thresholds. These
 124 preliminary triggers are then combined with the scintillator triggers to form the fi-
 125 nal electron and pion triggers, which are then sent to scalers to record the event
 126 counts and offline used to form asymmetries $A = (n_R - n_L)/(n_R + n_L)$, where
 127 $n_{R(L)}$ is the integrated rate of the triggers normalized to the integrated beam charge
 128 for the right(*R*) and left(*L*) handed spin (helicity) states of the incident electron
 129 beam. The scalers that count triggers and beam charge are integrated over the he-
 130 licity period, which was flipped pseudo-randomly at 30 Hz per the experimental
 131 technique used by the HAPPEX experiments [9].

132 For HRS the two layers of the lead-glass detector are called “preshower” and

133 “shower” detectors, respectively. The preshower blocks in the Right HRS (the spec-
 134 trometer located to the right side of the beamline when viewed along the beam
 135 direction) has 48 blocks arranged in a 2×24 array, with the longest dimension
 136 of the blocks aligned perpendicular to the particle trajectory. For the two blocks
 137 in each row, only the ends facing outward are read out by photo-multiplier tubes
 138 (PMTs) and the other ends of the two blocks were facing each other and not read
 139 out. Therefore the preshower detector had 48 output channels. All preshower blocks
 140 were individually wrapped to prevent light leak. The preshower and the shower de-
 141 tectors in the Left HRS are similar to the preshower detector on the Right HRS
 142 except that for each detector there are 34 blocks arranged in a 2×17 array. The
 143 shower detector in the Right HRS had 75 blocks arranged in a 5×15 array with the
 144 longest dimension of the blocks aligned along the trajectory of scattered particles.
 145 PMTs are attached to each block of the Right shower detector on one end only,
 146 giving 75 output channels.

147 Because the lead-glass detectors in the Left and Right HRS were different, design
 148 of the lead-glass-based triggers of the DAQ is also different, as shown in Fig. 1. As
 149 a compromise between the amount of electronics needed and the rate in the front
 150 end logic modules, the lead-glass blocks in both the preshower and the shower de-
 151 tectors were divided into 6 (8) groups for the Left (Right) HRS, with each group
 152 consisting 8 blocks. On the Right HRS only 60 of the 75 shower blocks were used
 153 while the 15 blocks on the edge were not read out. The reduction on the HRS ac-
 154 ceptance due to not using these side blocks is negligible. Signals from the 8 blocks
 155 in each group were added using a custom-made analog summing unit called the
 156 “SUM8 module”, then passed to discriminators. The geometry and the position of
 157 each preshower group were carefully chosen to match those of the corresponding
 158 shower group to maximize electron detection efficiency. On the Left HRS adjacent
 159 groups in both preshower and shower had overlapping blocks, while for the Right
 160 HRS only preshower blocks were overlapping. To allow overlap between adjacent
 161 groups, signals from preshower blocks on the Right HRS and from both preshower
 162 and shower blocks on the Left HRS were split into two identical copies using pas-
 163 sive splitters.

164 A schematic diagram for the DAQ electronics for the Right HRS is shown in Fig. 2.
 165 Preliminary electron and pion triggers were formed by passing shower (SS) and
 166 preshower (PS) signals or their sums, called total shower (TS) signals, through
 167 discriminators with different thresholds. For electron triggers, logical ANDs of the
 168 PS discriminator and the TS discriminator outputs were used. For pion triggers, low
 169 threshold discriminators on the TS signal alone were used to reject background.
 170 These preliminary triggers were then combined with signals from scintillators and
 171 the gas Cherenkov (called electron or pion “VETO” signals) to form electron or
 172 pion triggers for each shower and preshower group. The electron VETO signals
 173 required the gas Cherenkov to be triggered, while the pion VETO required the
 174 opposite. All six (eight) group electron or pion triggers on the Left (Right) HRS
 175 were then ORed together to form the global electron or pion trigger for the Left

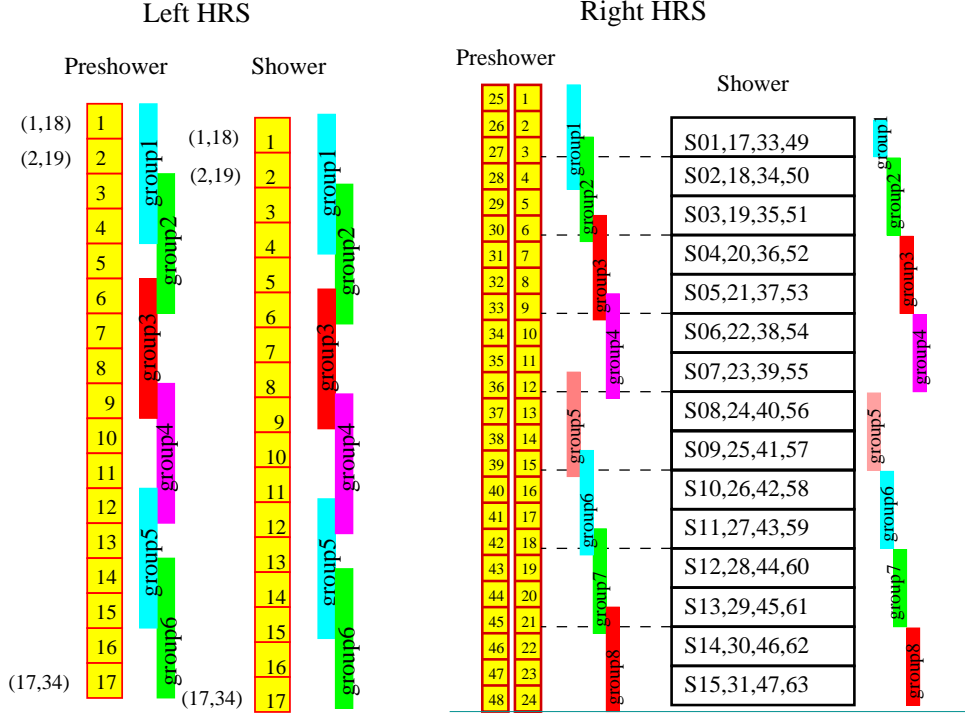


Fig. 1. [Color online] Grouping scheme (side-view) for the double-layer lead-glass detectors for the Left and the Right HRS. Scattered particles enter the detector from the left. The colored vertical bars represent the range of each group.

(Right) HRS. All group and the final electron and pion triggers were counted using scalars. Because pions do not produce large enough lead-glass signals to trigger the high threshold TS discriminators for the electron triggers, pions do not introduce extra counting deadtime for the electron triggers.

In order to monitor the counting deadtime of the DAQ, two identical paths of electronics were constructed. The only difference between the two paths is in the discriminator output width, set at 30 ns and 100 ns for the “narrow” and the “wide” paths, respectively. The scalars are rated for 250 MHz (4 ns deadtime) and therefore do not add to the deadtime. In addition, since the output width of all logic modules were set to 15 ns, the deadtime of the DAQ for each group is dominated by the deadtime of the discriminators.

The SUM8 modules used for summing all lead-glass signals also served as fan-out modules, providing exact copies of the input PMT signals. These copies were sent to the standard HRS DAQ for calibration. During the experiment, data were collected at low rates using reduced beam currents with both DAQs functioning, such that a direct comparison of the two DAQs can be made. The vertical drift chambers were used during these low rate DAQ studies. Outputs from all discriminators, signals from the scintillator and the gas Cherenkov, and all electron and pion group and global triggers were sent to Fastbus TDCs (fbTDC) and were recorded in the standard DAQ. Data from these fbTDCs were used to align amplitude spectrum

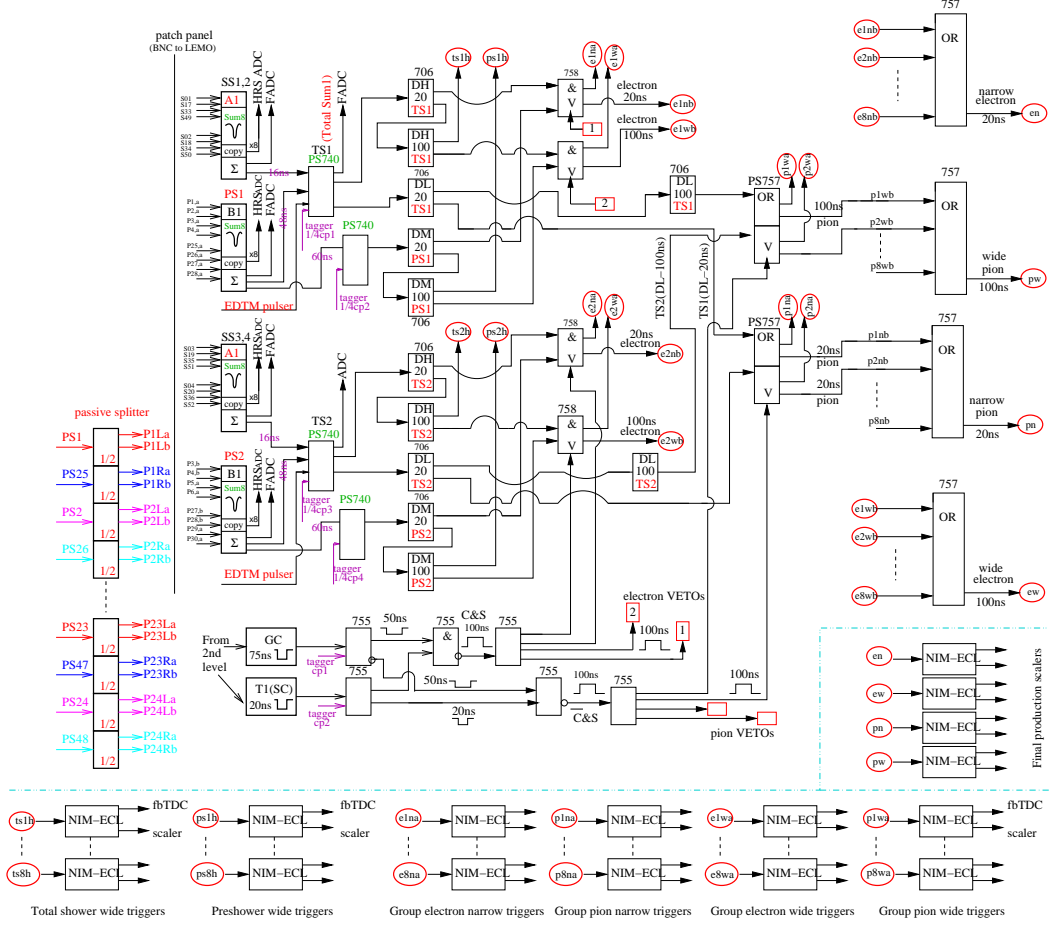


Fig. 2. [Color online] Electronics diagram for the Right HRS DAQ used by the PVDIS experiment. The Sum8's, discriminators and logic modules for two groups are shown, as well as the location of tagger signal inputs, setup of the VETO circuit using scintillator (SC) and gas Cherenkov (GC) signals, the logic units for combining triggers from all eight groups into final triggers, and the counting scalars. Electronics for the Left HRS are similar except for the grouping scheme.

and timing of all signals. They also allow the study of the Cherenkov or lead-glass detector performance for the new DAQ triggers.

Full sampling of partial analog signals were done using Flash-ADCs (FADCs) at low rates intermittently during the experiment. For one group on the left and one group on the right HRS, the preshower and shower SUM8 outputs, the intermediate logical signals of the DAQ, and the output electron and pion triggers were recorded. These FADC data provided a study of pileup effects to confirm the simulation and to provide the input parameters for the simulation, specifically the rise and fall times of the signals and their widths.

205 3 DAQ PID Performance

206 PID performance of the DAQ system was studied with calibration runs taken at low
 207 beam currents using fbTDC signals along with ADC data of all detector signals
 208 recorded by the standard DAQ. Events that triggered the DAQ would appear as a
 209 timing peak in the corresponding fbTDC data of the standard DAQ and a cut on this
 210 peak can be used to select those events. Figure 3 shows the preshower vs. shower
 211 signals for group 2 on the Left HRS. A comparison between no fbTDC cut and with
 212 cut on the fbTDC signal of the electron wide trigger from this group clearly shows
 the hardware PID cuts.

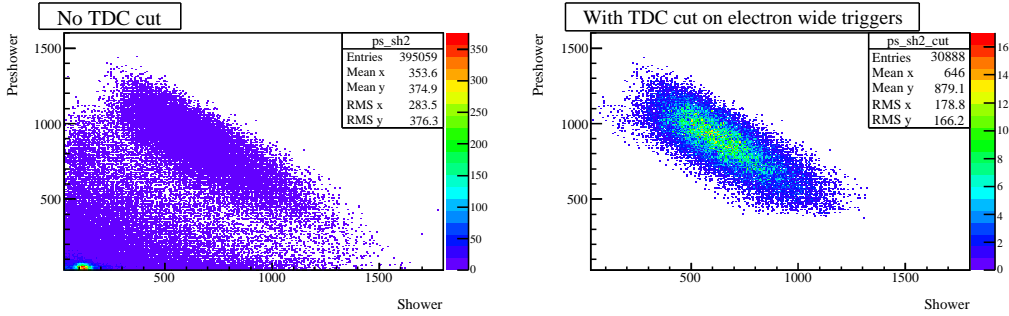


Fig. 3. [Color online] Preshower vs. Shower ADC data (sum of 8 blocks each) for group 2 on the Left HRS, without the fbTDC cut (left panel) and with cut on the group 2 electron wide trigger fbTDC signal (right panel). It clearly shows the thresholds on the preshower and the total shower signals, indicating the DAQ is selecting the correct events as electrons.

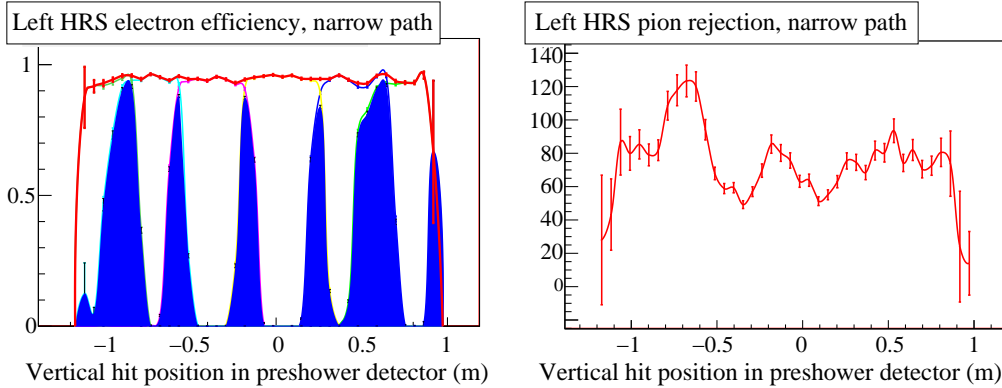


Fig. 4. [Color online] Electron detection efficiency (left) and pion rejection factor (right) vs. vertical (dispersive) hit position of the particle in the preshower detector for the narrow electron triggers in the Left HRS. A one-hour run was used in this evaluation. For electron efficiencies, the total efficiency is shown by the red curve, while blue shaded area indicates events that are recorded by the two adjacent groups. The average electron efficiency achieved by the lead glass detector alone for this one-hour run is $(94.626 \pm 0.002)\%$ and the average pion rejection factor is $(75.3 \pm 1.1) : 1$. The error bars are statistical only. PID performance for the wide path and the Right HRS are similar.

214 Electron efficiency and pion rejection factors of the lead-glass detector on the Left

215 HRS during a one-hour run are shown in Fig. 4 as functions of the location of the hit
 216 of the particle in the preshower detector. PID performance on the Right HRS is sim-
 217 ilar. Electron efficiency from wide groups are slightly higher than narrow groups
 218 because there is less event loss due to timing mis-alignment when taking the coinci-
 219 dence between the preshower and the total shower discriminator outputs. Variations
 220 in the electron efficiency across the spectrometer acceptance effectively influence
 221 the kinematics (Q^2) of the measurement. For this reason, low-rate calibration data
 222 were taken daily during the experiment to monitor the DAQ PID performance and
 223 corrections were applied to the asymmetry data.

224 The gas Cherenkov detector consists of 10 PMTs on both the Left and the Right
 225 HRS. Signals from all 10 PMTs were summed in an analog-sum module and sent to
 226 a discriminator. The discriminator output was sent to the DAQ (as shown in Fig. 2)
 227 as well as fbTDCs. Figure 5 shows the Cherenkov ADC sum with and without the
 fbTDC cut which clearly shows the capability of rejecting pions.

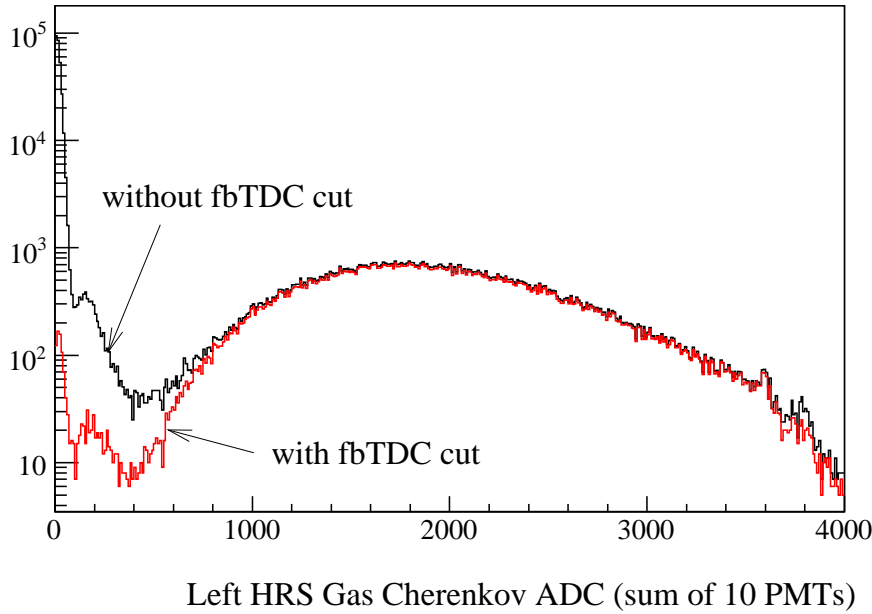


Fig. 5. [Color online] Cherenkov ADC data (sum of 10 PMTs) for the Left HRS, with a fbTDC cut on the Cherenkov discriminator output (red) and without (black). The discriminator clearly selected electrons while rejecting pions.

228

229 The electron detection efficiency and pion rejection factor averaged throughout the
 230 experiment are shown in Table 1 for different kinematics and for the Left and the
 231 Right HRS separately.

232 As described in the Introduction, pion contamination in the electron trigger would
 233 affect the measured electron asymmetry as $A_m = (1 - f)A_e + fA_\pi$ where A_m
 234 and A_e are the measured and the true electron asymmetries, respectively, f is the

Table 1

Average electron detection efficiency and pion rejection factor achieved through the lead glass (LG) and the gas Cherenkov (GC) detectors, respectively, and the combined performance. The error bars are statistical only.

Electron Detection Efficiency			
	$Q^2 = 1.1 \text{ (GeV/c)}^2$	$Q^2 = 1.9 \text{ (GeV/c)}^2$	
HRS	Left	Left	Right
LG	$(91.93 \pm 0.04)\%$	$(94.50 \pm 0.06)\%$	$(94.36 \pm 0.04)\%$
GC	$(99.14 \pm 0.02)\%$	$(99.03 \pm 0.03)\%$	$(98.19 \pm 0.06)\%$
combined	$(91.14 \pm 0.04)\%$	$(93.58 \pm 0.06)\%$	$(92.65 \pm 0.07)\%$
Pion Rejection			
	$Q^2 = 1.1(\text{GeV/c})^2$	$Q^2 = 1.1(\text{GeV/c})^2$	
HRS	Left	Left	Right
LG	$(101.5 \pm 1.6) : 1$	$(78.9 \pm 0.9) : 1$	$(72.7 \pm 0.3) : 1$
GC	$(158.6 \pm 3.5) : 1$	$(301.2 \pm 5.2) : 1$	$(414.3 \pm 6.2) : 1$
combined	$[(1.61 \pm 0.04) \times 10^4] : 1$	$[(2.38 \pm 0.05) \times 10^4] : 1$	$[(3.01 \pm 0.05) \times 10^4] : 1$

pion contamination fraction in the electron trigger, and A_π is the parity violation asymmetry of pion production. As shown in table 1, combined pion rejection factor from the lead-glass and the gas Cherenkov detector was above 10^4 throughout the experiment. The pion to electron rate ratios for the two Q^2 values of this experiment were less than 10:1, thus $f < 10/10^4 = 10^{-3}$. Because pions are produced from nucleon resonance decays, the parity violation asymmetry of pion production is expected to be no larger than that of scattered electrons with the same momentum. This was confirmed by asymmetries formed from pion triggers during this experiment. Overall the uncertainty in the electron asymmetry due to pion contamination is less than 10^{-3} and is negligible compared to the 3 – 4% statistical uncertainty.

4 DAQ Deadtime

Deadtime is the amount of time after an event during which the system is unable to record another event. Identifying the exact value of the deadtime is always a challenge in counting experiments. By having a narrow and wide path, we can observe the trend in the deadtime – the wider path should have higher deadtime. By matching the observed trend with our simulation we can benchmark and confirm the simulation result of our deadtime. In addition, dividing lead-glass blocks into groups greatly reduces the deadtime loss in each group compared to summing all blocks together and forming only one final trigger.

254 To illustrate the importance of the deadtime, consider its effect on the asymmetry
 255 A . For a simple system with only one contribution to the deadtime δ , the observed
 256 asymmetry A_O is related to the true asymmetry A according to $A_O = (1 - \delta)A$. In
 257 this experiment δ was on the order of 0.02 (dependent on the rate). To achieve a 3%
 258 accuracy on the asymmetry, δ must be known with a $\leq 30\%$ relative accuracy, so
 259 that it becomes a negligible systematic error. The DAQ we deployed was, however,
 260 more complex, having the three contributions to the deadtime, as listed below and
 261 shown in Fig. 2:

- 262 (1) The “group” deadtime: deadtime due to discriminators and logical AND mod-
 263 ules used to form group triggers;
- 264 (2) The “veto” deadtime: deadtime from electronics that used scintillator and
 265 Cherenkov signals to form the “gate” signals which were sent to the AND
 266 module of each group to form group electron and pion triggers.
- 267 (3) The “OR” deadtime: deadtime due to the logical OR module when combining
 268 all group triggers.

269 The final deadtime is a combination of all three. In order to evaluate the DAQ
 270 deadtime, a full-scale simulation was developed as follows: The analog signals for
 271 preshower, shower, scintillator and gas Cherenkov as recorded by ADCs from low-
 272 current runs are fed to the simulation as inputs. The simulation takes into account all
 273 electronics and delay cables of the DAQ and calculate digital outputs from discrim-
 274 inators, all AND and OR modules. For the preshower and shower SUM8 outputs,
 275 FADC data were used to determine the signal width.

276 4.1 Group Deadtime Measurement

277 In order to study the group deadtime, a high rate pulser signal (“tagger”) was mixed
 278 with the Cherenkov and all preshower and total shower signals using analog sum-
 279 ming modules, see Figs. 2 and 6. In the absence of all detector signals, a tagger
 280 pulse produces without loss an electron trigger output, and a “tagger-trigger co-
 281 incidence” pulse between this output and the “delayed tagger” – the tagger itself
 282 with an appropriate delay to account for the DAQ response time. When high-rate
 283 detector signals are present, however, some of the tagger pulses would not be able
 284 to trigger the DAQ due to deadtime. The relative loss in the electron trigger output
 285 w.r.t. the tagger input has two components:

- 286 (1) The count loss R_o/R_i : when a detector PMT signal precedes the tagger signal
 287 by a time interval δt shorter than the DAQ deadtime but longer than $w + t_1$, the
 288 tagger signal is lost and no coincidence output is formed. Here w is the width
 289 of the trigger output and t_1 is the time interval the delayed tagger precedes
 290 the tagger’s own trigger output, see Fig. 6. During the experiment w was set
 291 to 15 ns for all groups, t_1 was measured at the end of the experiment and was

found to be between 20 and 40 ns.

- (2) The pileup fraction p : when a PMT signal precedes the tagger signal by a time interval δt shorter than $w + t_1$, there would be coincidence output between the delayed tagger and the electron output triggered by the detector PMT signal. If furthermore δt is less than the DAQ deadtime (which is possible for this experiment since the deadtime is expected to be as long as 100 ns for the wide path), the tagger itself is lost due to deadtime and the tagger-trigger coincidence is a false count and should be subtracted. In the case if δt is shorter than $w + t_1$ but longer than the DAQ deadtime (not possible for this experiment but could happen in general), the tagger itself also triggers a tagger-trigger coincidence but in this case, there are two tagger-trigger coincidence events, both recorded by the fbTDC if working in the multi-hit mode, and one is a false count and should be subtracted.

The pileup effect can be measured using the delay between the coincidence output and the input tagger. This is illustrated in Fig. 6 and the pileup effect contributes to both I_1 and I_2 regions of the fbTDC spectrum. Fractions of I_1 and I_2 relative to I_0 are expected to be $I_1/I_0 = Rt_1$ and $I_2/I_0 = Rw$, respectively, where R is the PMT signal rate. The pileup effect was measured using fbTDC spectrum for electron narrow and wide triggers for all groups. Data for $I_{1,2}$ extracted from fbTDC agree very well with the expected values.

The relative loss of tagger events due to DAQ deadtime is evaluated as

$$D = 1 - (1 - p)(R_o/R_i), \quad (3)$$

where R_i is the input tagger rate, R_o is the output tagger-trigger coincidence rate, and $p = (I_1 + I_2)/I_0$ is a correction factor for pileup effects as defined in Fig. 6. Results for the deadtime loss D are shown in Figs. 7 and 8, for group 4 on the left HRS and group 4 on the right HRS, respectively, and are compared with simulation. Different beam currents between 20 and 100 μA were used in this dedicated deadtime measurement. In order to reduce the statistical fluctuation caused by limited number of trials in the simulation within a realistic computing time, simulations were done at higher rates than the actual measurement.

The slope of the tagger loss vs. event rate gives the value of group deadtime in seconds, as shown in Figs. 7 and 8. One can see that the deadtime for the wide path is approximately 100 ns as expected. The deadtime for the narrow path, on the other hand, is dominated by the input PMT signal width (typically 60-80 ns) instead of the 30-ns discriminator width. The simulated deadtime agree very well with data for both HRSs and for both wide and narrow paths.

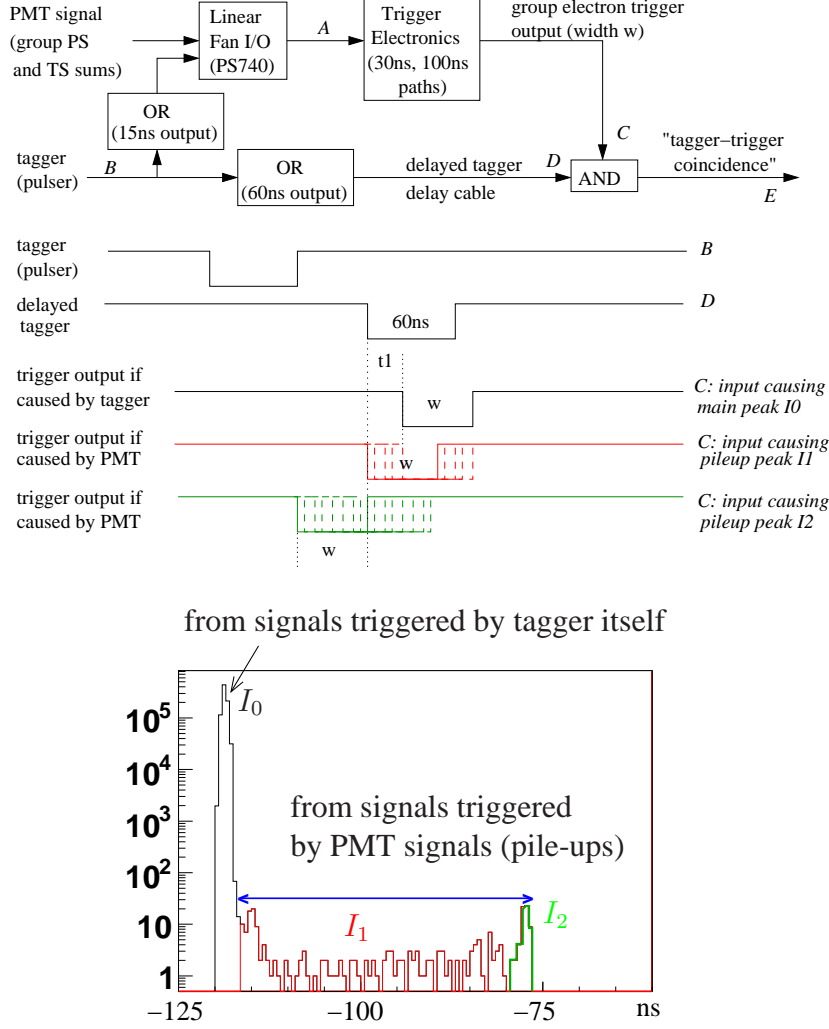


Fig. 6. [Color online] Top: schematic diagram for the tagger setup and signal timing sequence. The two logical OR units immediately following the tagger input “B” serve as width adjusters. Bottom: fbTDC spectrum for the relative timing between tagger-trigger coincidence and the input tagger, in 0.5-ns bins. The fbTDC module works in the multi-hit mode. Two different scenarios are shown: 1) Main peak I_0 : when there is no PMT signal preceding the tagger, the tagger triggers the DAQ and forms a tagger-trigger coincidence. 2) Pileup events I_1 and I_2 : when there is a PMT signal preceding the tagger by a time interval shorter than $w + t_1$, the PMT signal triggers the DAQ and forms a tagger-trigger coincidence signal with the delayed tagger.

326 4.2 Total Deadtime Evaluation

327 Although the deadtime loss of each group was measured using tagger signals, the
 328 dominating term in the total deadtime is from the veto electronics because the to-
 329 tal trigger rate from scintillators and gas Cherenkov is much higher than individ-
 330 ual group rates. The difference in total loss between narrow and wide path is thus

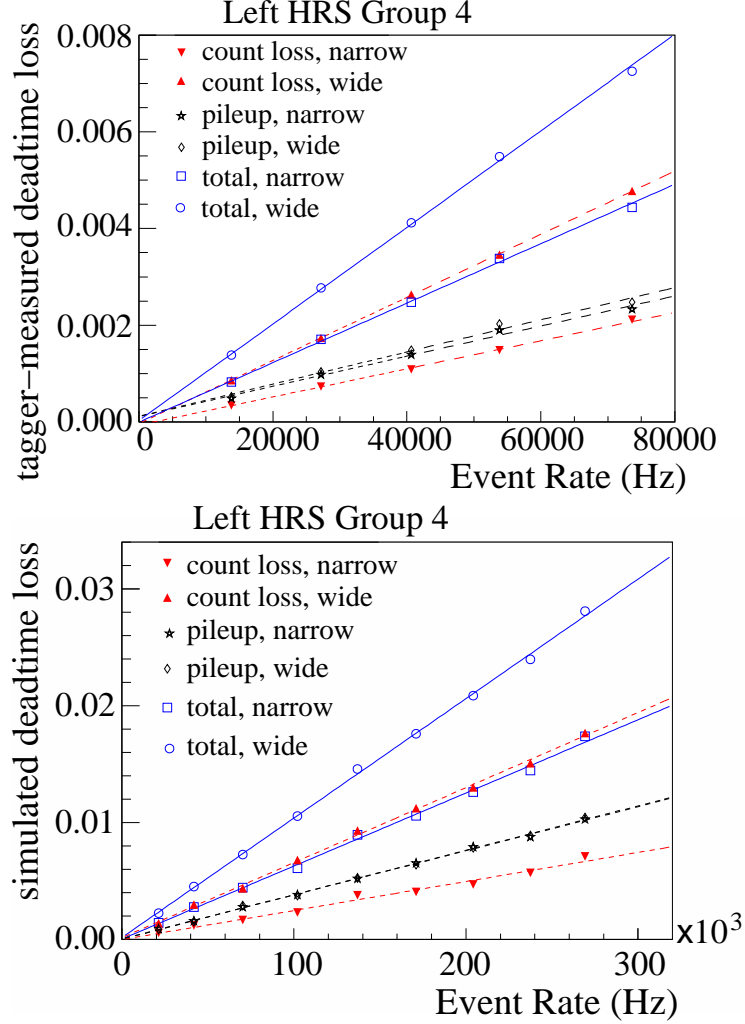


Fig. 7. [Color online] Deadtime loss in percent vs. event rate from the tagger method for group 4 on the Left HRS. Top: actual deadtime loss from tagger measurements; Bottom: simulated deadtime loss of the tagger. The tagger fractional count loss $1 - R_o/R_i$ (red) and the pileup correction p (black) are combined to form the total group deadtime D (blue). These data were taken (or simulated) at a Q^2 of 1.1 (GeV/c)^2 . To minimize the statistical uncertainty while keeping the computing time reasonable, the simulation used higher event rates than the tagger measurement. The total group deadtime can be determined from the linear fit slope coefficients: tagger data narrow $p_1 = (61.5 \pm 0.2) \times 10^{-9} \text{ s}$, wide $p_1 = (99.9 \pm 0.3) \times 10^{-9} \text{ s}$, simulation narrow $p_1 = (62.5 \pm 1.4) \times 10^{-9} \text{ s}$, wide $p_1 = (102 \pm 1.3) \times 10^{-9} \text{ s}$. Group 4 is from the central blocks of the lead-glass detector and has the highest rate among all groups.

331 smaller than that in their group deadtimes. Simulation for the veto deadtime was
 332 compared with FADC data and the agreement was found to be at 20% level or bet-
 333 ter. After subtracting group and veto deadtimes from the total simulated deadtime,
 334 the remaining is attributed to the logical OR module. There is no direct measure-
 335 ment of the logical OR deadtime, but the effect of the logical OR module is quite
 336 straightforward and can be calculated analytically. The difference between the sim-

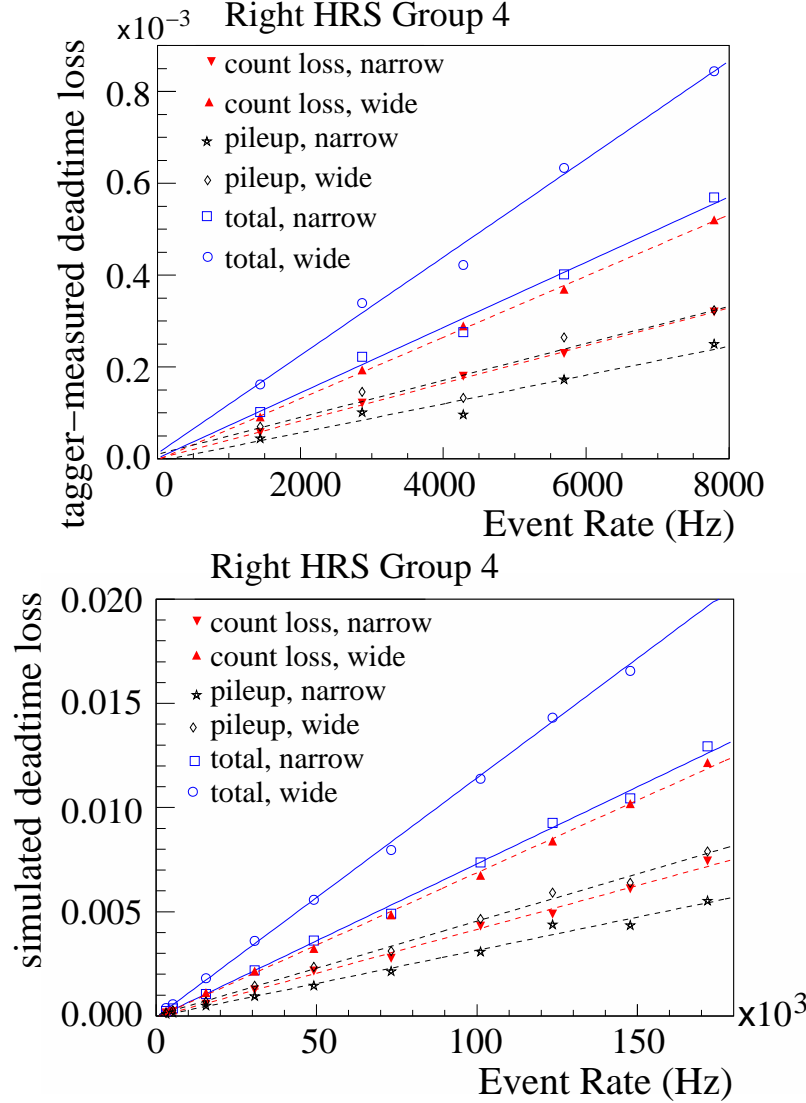


Fig. 8. [Color online] Deadtime loss in percent vs. event rate from the tagger method for group 4 on the Right HRS. Top: tagger data; Bottom: simulation. These data were taken (or simulated) at a Q^2 of 1.9 (GeV/c) 2 . The total group deadtime can be determined from the linear fit slope coefficients: tagger data narrow $p_1 = (71.1 \pm 0.9) \times 10^{-9}$ s, wide $p_1 = (107 \pm 1.2) \times 10^{-9}$ s, simulation narrow $p_1 = (73.9 \pm 1.5) \times 10^{-9}$ s, wide $p_1 = (115 \pm 1.5) \times 10^{-9}$ s. Group 4 is from the central blocks of the lead-glass detector and has the highest rate among all groups. See Fig. 7 caption for details.

337 ulation and the analytic results was used to estimate the uncertainty of the OR
338 deadtime.

339 The simulated deadtime loss of the global electron triggers and its decomposi-
340 tion into group, veto, and OR are shown in Table 2. The total deadtime is also
341 shown in Fig. 9 as a function of the total event rate. The deadtime corrections
342 to the final asymmetry results from the wide path triggers are $(1.64 \pm 0.16)\%$
343 and $(0.931 \pm 0.215)\%$, for $Q^2 = 1.1$ and 1.9 (GeV/c) 2 , respectively. These pro-

Table 2

Simulated DAQ deadtime loss (in percent) and fractional contributions from group, veto, and OR deadtimes. The fractional deadtime from OR is calculated as one minus those from group and veto, and its uncertainty is estimated from the difference between simulation and the analytical results. The uncertainty of the total deadtime is the uncertainties from group, veto and OR added in quadrature.

Q^2 (GeV/c) ²	Path	fractional contribution			Total deadtime loss at 100 μ A
		Group	Veto	OR	
1.1	narrow	(20.6 \pm 2.1)%	(51.3 \pm 1.9)%	(28.1 \pm 8.6)%	(1.45 \pm 0.13)%
	wide	(29.5 \pm 2.4)%	(45.3 \pm 1.7)%	(25.3 \pm 9.0)%	(1.64 \pm 0.16)%
1.9	narrow	(2.9 \pm 0.2)%	(80.6 \pm 18.5)%	(16.5 \pm 12.3)%	(0.885 \pm 0.196)%
	wide	(4.3 \pm 0.4)%	(76.6 \pm 17.5)%	(19.1 \pm 15.1)%	(0.931 \pm 0.215)%

vide a direct correction to the measured asymmetry and the uncertainties are small compared to other dominant systematic uncertainties such as the beam polarization measurement.

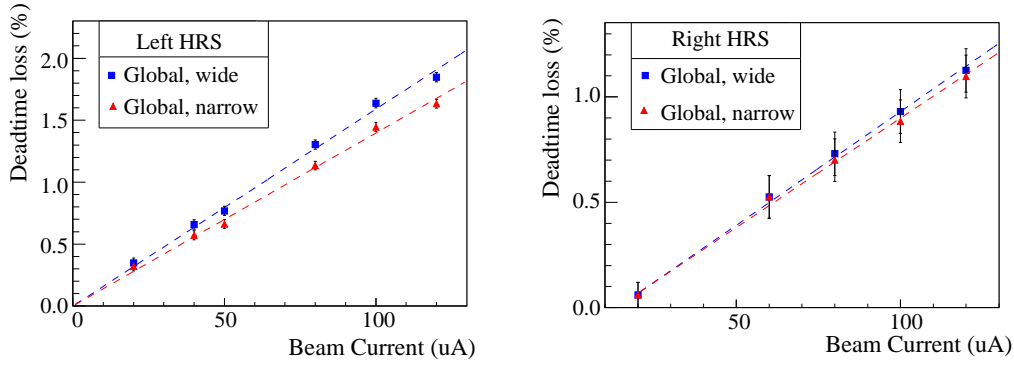


Fig. 9. [Color online] Simulated deadtime loss of the global electron trigger for the Left (left) and the Right (right) HRS. The error bars shown are due to statistical uncertainty of the simulation. See Table 2 for final uncertainty evaluation.

4.3 Asymmetries

The physics asymmetries sought for in this experiment are 91 and 160 ppm, for $Q^2 = 1.1$ and 1.9 (GeV/c)², respectively. The measured asymmetries are about 90% of these values due to beam polarization. To understand the systematics of the asymmetry measurement, a half-wave plate (HWP) was inserted in the beamline to flip the laser helicity in the polarized source during half of the data taking period. The measured asymmetries flip sign for each beam HWP change and the magnitude of the asymmetry remain consistent within statistical error bars.

The asymmetries can be formed from event counts of each beam helicity pair, with

356 33-ms of helicity right and 33-ms of helicity left beam, normalized by the beam
 357 charge. Figure 10 shows the pull distribution of pair-wise asymmetries with the
 358 “pull” defined as

$$p_i \equiv (A_i - \langle A \rangle) / \delta A_i , \quad (4)$$

359 where A_i is the asymmetry extracted from the i -th beam helicity pair with the HWP
 360 states already corrected and $\delta A_i = 1/\sqrt{N_i^R + N_i^L}$ its statistical uncertainty with
 361 $N_i^{R(L)}$ the event counts from the right (left) helicity pulse of the pair, and $\langle A \rangle$ is the
 362 asymmetry averaged over all beam pairs. One can see that the asymmetry spectrum
 363 agrees to five orders of magnitude with Gaussian distribution expected from purely
 364 statistical fluctuations.

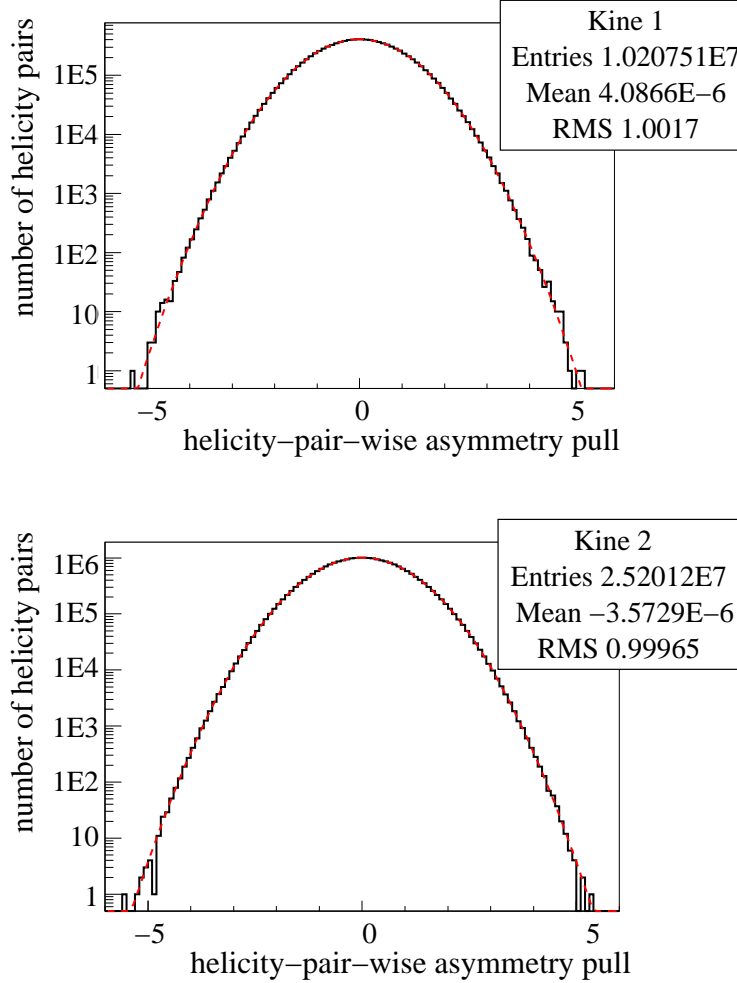


Fig. 10. [Color online] Pull distribution [Eq.(4)] for the global electron narrow trigger for $Q^2 = 1.1$ (top) and $Q^2 = 1.9$ (GeV/c)² (bottom).

365 5 Summary

366 A scaler-based counting DAQ with hardware-based particle identification was suc-
367 cessfully implemented in the 6 GeV PVDIS experiment at Jefferson Lab. Asymme-
368 tries measured by the DAQ follow Gaussian distributions as expected from purely
369 statistical measurements. Particle identification performance of the DAQ were mea-
370 sured and corrections are applied to the data on a day-to-day basis. The overall pion
371 rejection achieved was better than $(1.6 \times 10^4) : 1$ with an electron efficiency above
372 91% throughout the experiment, and the systematic uncertainty on the asymme-
373 try due to pion background is below 10^{-3} . DAQ deadtime was calculated from a
374 full-scale timing simulation and contributes a $\approx 0.2\%$ systematic uncertainty to
375 the final asymmetry results and are negligible compared to the $(3 - 4)\%$ statisti-
376 cal uncertainty and other leading systematic uncertainties. Results presented here
377 demonstrate that accurate asymmetry measurements can be performed with even
378 higher event rates or backgrounds with this type of scaler-based DAQ.

379 Acknowledgments

380 This work is supported in part by the Jeffress Memorial Trust under Award No.
381 J-836, the U.S. National Science Foundation under Award No. 0653347, and the
382 U.S. Department of Energy under Award No. DE-SC0003885. **Notice:** Authored
383 by Jefferson Science Associates, LLC under U.S. DOE Contract No. DE-AC05-
384 06OR23177. The U.S. Government retains a non-exclusive, paid-up, irrevocable,
385 world-wide license to publish or reproduce this manuscript for U.S. Government
386 purposes.

387 References

- 388 [1] JLab experiment E08-011 (previously E05-007), R. Michaels, P.E. Reimer and X.-C.
389 Zheng, spokespersons.
- 390 [2] R. Subedi *et al.*, AIP proceedings of the 18th International Spin Physics Symposium
391 (2009) 245.
- 392 [3] J. Alcorn *et al.*, Nucl. Instrum. Meth. **A522** (2004) 294.
- 393 [4] R. Hasty *et al.* [SAMPLE Collaboration], Science **290**, 2117 (2000) [nucl-
394 ex/0102001].
- 395 [5] K. A. Aniol *et al.* [HAPPEX Collaboration], Phys. Rev. C **69**, 065501 (2004) [nucl-
396 ex/0402004].

- 397 [6] A. Acha *et al.* [HAPPEX Collaboration], Phys. Rev. Lett. **98**, 032301 (2007) [nucl-
398 ex/0609002].
- 399 [7] K. A. Aniol *et al.* [HAPPEX Collaboration], Phys. Rev. Lett. **96**, 022003 (2006) [nucl-
400 ex/0506010].
- 401 [8] K. A. Aniol *et al.* [HAPPEX Collaboration], Phys. Lett. B **635**, 275 (2006) [nucl-
402 ex/0506011].
- 403 [9] Z. Ahmed *et al.* [HAPPEX Collaboration], Phys. Rev. Lett. **108**, 102001 (2012)
404 [arXiv:1107.0913 [nucl-ex]].
- 405 [10] S. Abrahamyan, Z. Ahmed, H. Albataineh, K. Aniol, D. S. Armstrong, W. Armstrong,
406 T. Averett and B. Babineau *et al.*, Phys. Rev. Lett. **108**, 112502 (2012)
407 [arXiv:1201.2568 [nucl-ex]].
- 408 [11] C.Y. Prescott *et al.*, Phys. Lett. **B77** (1978) 347.
- 409 [12] C.Y. Prescott *et al.*, Phys. Lett. **B84** (1979) 524.
- 410 [13] F. E. Maas *et al.* [A4 Collaboration], $Q^2 = 0.230-(\text{GeV}/c)^2$, Phys. Rev. Lett. **93**,
411 022002 (2004) [nucl-ex/0401019].
- 412 [14] F. E. Maas, K. Aulenbacher, S. Baunack, L. Capozza, J. Diefenbach, B. Glaser,
413 T. Hammel and D. von Harrach *et al.*, $Q^2 = 0.108 (\text{GeV}/c)^2$, Phys. Rev. Lett.
414 **94**, 152001 (2005) [nucl-ex/0412030].
- 415 [15] S. Baunack, K. Aulenbacher, D. Balaguer Rios, L. Capozza, J. Diefenbach,
416 B. Glaser, D. von Harrach and Y. Imai *et al.*, Phys. Rev. Lett. **102**, 151803 (2009)
417 [arXiv:0903.2733 [nucl-ex]].
- 418 [16] D. H. Beck, Phys. Rev. D **39**, 3248 (1989).
- 419 [17] D. S. Armstrong *et al.* [G0 Collaboration], Phys. Rev. Lett. **95**, 092001 (2005) [nucl-
420 ex/0506021].
- 421 [18] D. Androic *et al.* [G0 Collaboration], Phys. Rev. Lett. **104**, 012001 (2010)
422 [arXiv:0909.5107 [nucl-ex]].
- 423 [19] D. Marchand, J. Arvieux, G. Batigne, L. Bimbot, A. S. Biselli, J. Bouvier, H. Breuer
424 and R. Clark *et al.* Nucl. Instrum. Meth. A **586**, 251 (2008) [nucl-ex/0703026 [NUCL-
425 EX]].
- 426 [20] D. Androic *et al.* [G0 Collaboration], Nucl. Instrum. Meth. A **646**, 59 (2011)
427 [arXiv:1103.0761 [nucl-ex]].